PROCEEDINGS, 51st Workshop on Geothermal Reservoir Engineering
Stanford University, Stanford, California, February 9-11, 2026
SGP-TR-230

Stochastic Assessment of Lithium and Geothermal Co-resources in the Northern Smackover Formation

Bulbul Ahmmed[1], Alamgir Hosain[1,2], Chelsea Neil[1], Mohamed Mehana[1]

[1]Earth and Environmental Sciences Division, Los Alamos, New Mexico 87545

[2]University of Memphis, Memphis, Tennessee 38152

ahmmedb@lanl.gov

Keywords: Smackover, Direct Lithium Extraction, Lithium and Geothermal Co-resources, Geothermal

ABSTRACT

The Smackover Formation in the southern United States has recently emerged as a promising reservoir for lithium (Li) hosted in subsurface brines, with opportunities for co-production alongside geothermal energy. This study develops a stochastic assessment of lithium and geothermal resource potential in the northern Smackover using publicly available brine chemistry datasets that span both lateral and vertical sampling depths. Variogram analyses quantify spatial continuity, revealing long horizontal correlation ranges (10-40 km) but much shorter vertical ranges (250-1,000 m), which guided an anisotropic inverse distance weighting interpolation of Li concentration. The resulting 3D model delineates subsurface enrichment zones and yields an estimated seven million tonnes of total Li in-place across ~770 km^3 of reservoir volume. Incorporating stochastic distributions of porosity, oil–water contact, and extraction efficiency indicates that only ~0.3 million tonnes are realistically recoverable, with recoverability limited primarily by low effective porosity and non-uniform brine saturation. Geothermal potential was evaluated using an analytical enhanced geothermal systems framework that assumes parallel fracture flow and constant heat extraction over a 30-year plant lifetime. Temperature drawdown estimates between 2,300 and 2,600 m depth (12-21°C) were combined with stochastic sampling of seven thermophysical and operational parameters to compute power density. Thermodynamic maxima range from ~8 to 14 W m^{-2}, whereas realistic power densities cluster narrowly between 0.48 and 0.86 W m^{-2} due to low conversion efficiencies and modest geologic success factors. Together, these results highlight substantial Li endowment but modest geothermal potential and demonstrate the utility of stochastic co-resource assessment for informing future development strategies in the Smackover Formation.

---

1. INTRODUCTION

Li is one of the most critical minerals driving the global energy transition due to its extensive use in rechargeable Li-ion batteries for electric vehicles, portable electronics, grid-scale energy storage, and various industrial and medical applications (Swain, 2017). The global demand for lithium rose by nearly 30% in 2024, significantly exceeding the ~10% annual growth rate of the 2010s (IEA, 2025). A forecast from the IEA indicates lithium demand could rise by about five-fold compared to current levels by 2040 under certain scenarios, driven primarily by the electrification of transportation and renewable energy storage requirements (IEA, 2025). The U.S. Geological Survey (USGS) restored lithium as a critical mineral in the 2024 Critical Minerals List (USGS, 2024).

Globally, lithium is extracted through four primary pathways: 1) hard-rock mining, mainly from spodumene deposits in Australia and China; 2) continental brine extraction from evaporites in South America (Chile, Argentina, Bolivia); 3) subsurface brine recovery from geothermal and oilfield reservoirs; and 4) dilute lithium extraction from seawater (Flexer et al., 2018; He et al., 2020; Munk et al., 2016; Ruberti, 2024; Zhang et al., 2024). Hard-rock mining accounts for approximately 60-65% of global Li production, while continental brine sources contribute about 30-35% (Munk et al., 2016). As global lithium production is geographically concentrated, mainly in Australia, Chile, and China, the United States faces supply-chain vulnerabilities that may affect clean energy and high-tech manufacturing sectors (U.S. DEPARTMENT OF ENERGY, 2024). Consequently, identifying and developing domestic lithium resources, particularly from subsurface brines, has become a national priority.

The Smackover Formation in the U.S. Gulf Coast region, spanning southern Arkansas, eastern Texas, northern Louisiana, and western Mississippi, has recently attracted significant attention as a potential lithium-bearing brine reservoir (Gardner & Birdwell, 2025; Knierim et al., 2024; Moldovanyi et al., 1992). This carbonate formation, deposited during the Late Jurassic period, occurs at depths ranging approximately from 2,000 to 4,000 meters, with reservoir temperatures suitable for geothermal co-production (Knierim et al., 2024; Moldovanyi et al., 1992). Preliminary brine analyses from oil and gas wells in southern Arkansas and eastern Texas reveal lithium concentrations ranging from 100 to more than 400 mg/L, suggesting economically recoverable levels comparable to South American brine

deposits (Knierim et al., 2024; Peng Li, 2023). The region's dual potential for critical mineral extraction and geothermal energy recovery presents a unique opportunity for integrated development (Nondorf, 2016).

Previous studies have focused primarily on surface-level interpolations of Li concentration or regional geochemical mapping, which limits understanding of the three-dimensional (3D) distribution of lithium including depth (Huang et al., 2025; Knierim et al., 2024; Marza et al., 2024). These studies only mapped Li concentration on 2D maps, which cannot capture geochemical variability and stochasticity. Our study addresses these limitations by conducting variogram analyses of Li concentration along both horizontal and vertical directions and performing stochastic resources estimation through a Monte Carlo approach. Variogram analyses help define interpolation ranges that minimize error in 3D geospatial modeling (Dixit et al., 2024; Madalimov et al., 2025). Next, the interpolation ranges were used in inverse distance weighting (IDW) to estimate Li concentration within the interpolation range. Concentrations were left un-interpolated where there is no data within the interpolation range. Next, a total amount of Li resources was estimated in the study domain and stochasticity was introduced through porosity, oil water contact, and extraction efficiency.

For geothermal resource estimation, we applied an analytical framework to evaluate total heat in place, thermodynamic power potential, and both realistic maximum and minimum power densities across the study domain (Burns et al., 2025). These analytic solutions assume that the reservoir is sufficiently large for fracture spacing to be represented as an effective thermal medium i.e., the reservoir contains numerous hydraulically active fractures that contribute similarly to heat exchange, rather than one or two dominant fractures. Under this assumption, heat flow into a repeating pattern of fractures and adjacent conductive blocks can be replaced by the average volumetric heat supply. This representative thermal medium is then used to estimate the heat delivered from the fractured zone, which is combined with conductive recharge from the surrounding rock to quantify the total heat available for conversion to electricity. Here, stochasticity was brought up with seven parameters on rock, reservoir efficiency, and heat to power efficiency.

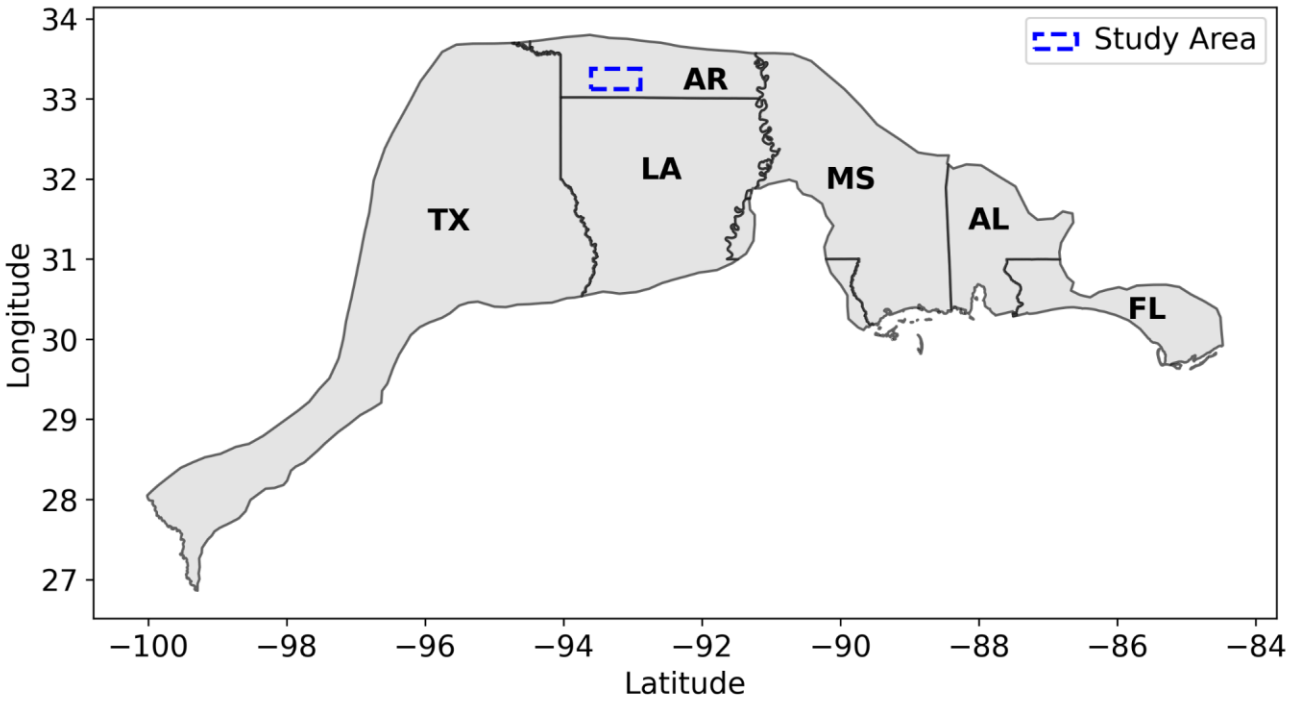

Figure 1: Study area (blue dashed rectangle) and the extent of Smackover formation in the Southern USA. The study area contains high Li concentration and high data frequency.

2. DATA

Lithium concentration data from deep brine wells across the southern United States were compiled for this study (Darvari et al., 2024; Marza et al., 2024; Attanasi et al., 2024; Knierim et al., 2024; Blondes et al., 2023). The study area includes 541 sampling locations with 18 measured variables, encompassing both lithium concentrations and geothermal attributes. Lithium was detected at all these points, delineating several zones of elevated resource potential. Spatial patterns of lithium enrichment and geothermal temperature within the Smackover Formation indicate three distinct hotspots favorable for co-production of lithium and geothermal energy (Huang et al., 2025). One major hotspot occurs in the northern Smackover Formation within southern Arkansas (AR), where high lithium concentrations (>83.97 mg/L) coincide with medium to high geothermal temperatures (≥100 °C). Geothermal data include temperature estimates from depths of 2 km to 7 km (Aljubran et al., 2024). Because the Smackover interval lies between approximately 2,300 and 2,600 m, data within this depth window were selected for analysis (Dickinson, 1968).

3. METHODS

The total Li reserve estimation workflow consists of (i) spatial continuity analysis using variograms, (ii) 3D interpolation using an anisotropic IDW method, (iii) total lithium reserve estimation, and (iv) introduction of stochasticity through uniform distribution of three parameters, including porosity, oil water contact ratio, and extraction efficiency (Figure 1). Geothermal resource potential or power density was evaluated using analytical equations for EGS (Burns et al., 2025). A total of seven parameters were sampled to estimate stochastic power density, including thermal conductivity (W/m/K), bulk density (kg/m³), specific heat capacity (J/kg/K), heat → electricity efficiency (-), geology heterogeneity success factor (-), temperature drawdown (°C), fracture spacing (m), and reservoir radius (m).

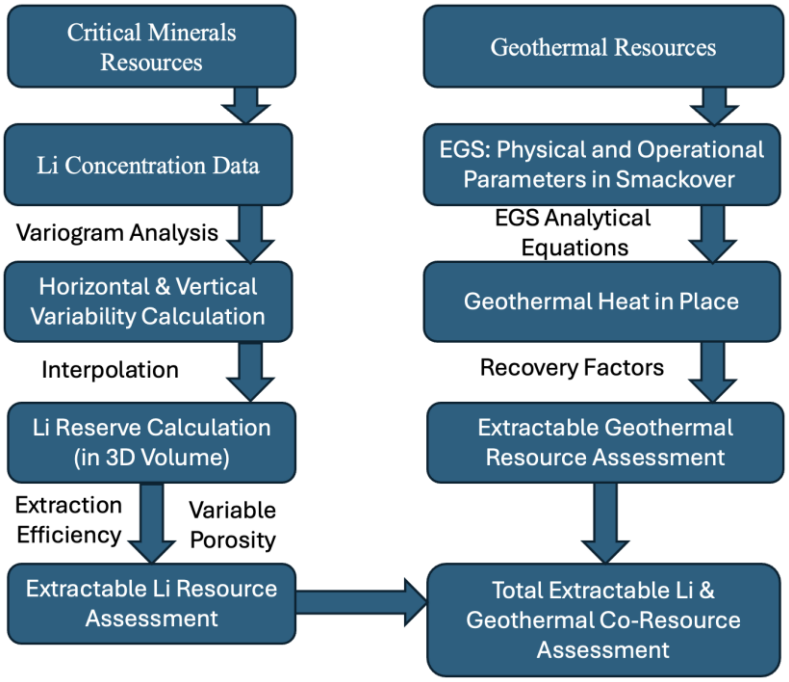

Figure 2: Workflow for assessing lithium and geothermal resource potential in brines of the Smackover Formation.

3.1 Variogram Analysis

Variogram analysis was performed to quantify spatial continuity and directional anisotropy in Li concentration within the study domain (Matheron, 1963; Journel & Huijbregts, 1978). The variogram, $\gamma(h)$, describes how the semi-variance between samples increases as a function of separation distance h, representing the degree of spatial correlation between points:

$$\gamma(h) = \frac{1}{2N(h)} \sum_{i=1}^{N(h)} [Z(x_i) - Z(x_i + h)]^2 \quad (1)$$

where $Z(x_i)$and $Z(x_i + h)$ are the measured Li concentrations at locations x_i and $x_i + h$, and *N(h)* is the number of sample pairs separated by lag distance h. The semi variogram generally increases with h until reaching a plateau, named as the sill, beyond which points are effectively uncorrelated. The distance at which this occurs is called range, while the nugget represents micro-scale variability and measurement noise observed as a discontinuity at the origin (Isaaks & Srivastava, 1989).

An omnidirectional horizontal variogram was computed using easting (m) and northing (m) coordinates to characterize the lateral variability of Li concentrations. Li concentration along depth was analyzed separately to characterize vertical variability of Li concentration. To minimize sampling bias, horizontally proximate samples (within 2 km) were grouped using density-based spatial clustering (DBSCAN; Ester et al., 1996), ensuring that vertical variability was derived from nearly co-located points. Both horizontal and vertical variograms were estimated using the Cressie-Hawkins robust estimator (Cressie & Hawkins, 1980) and fitted with standard theoretical models: spherical, exponential, and Gaussian (Isaaks & Srivastava, 1989).

The spherical model, which reaches the sill at a finite distance a is expressed as:

$$\gamma(h) = \begin{cases} c_0 + c\left[\frac{3h}{2a} - \frac{1}{2} \times \frac{3}{2}\left(\frac{h}{a}\right)^3\right], & 0 \le h \le a \\ c_0 + c, & h > a \end{cases} \quad (2)$$

The exponential model is described as:

$$\gamma(h) = c_0 + c\,(1 - e^{-h/a}) \quad (3)$$

Gaussian model is given by:

$$\gamma(h) = c_0 + c\,(1 - e^{-(h/a)^2}) \quad (4)$$

Where c_0 is the nugget, c is the structured sill, and a is the range. The horizontal variograms indicated correlation ranges of approximately 24-40 km, while the vertical detrended variograms showed much shorter ranges of 250-1,000 m (Table 1 & Figure 3). These radii ensure that interpolation reflects the anisotropic nature of the Smackover Formation, which displays strong lateral connectivity but sharp vertical gradients.

Table 1: Variogram analysis results using different models.

	Spherical Model			Exponential Model			Gaussian Model		
	Range (m)	Sill (m)	Nugget (m)	Range (m)	Sill (m)	Nugget (m)	Range (m)	Sill (m)	Nugget (m)
Horizontal Variogram (XY)	24304.26	26341.87	0.00	41396.33	28853.28	0.00	18781.66	26357.13	3924.11
Vertical Variogram (Z)	337.57	5458.35	1309.60	1101.59	8590.71	1412.01	245.56	5724.74	1760.67

Lithium concentrations increase or decrease systematically with depth due to temperature, salinity, and diagenetic effects. To isolate local-scale vertical variability, depth trends were removed prior to vertical variogram modeling by fitting a quadratic polynomial to the raw concentration-depth relationship:

$$v_{\text{trend}}(z) = k_0 + k_1 d + k_2 d^2 \quad (5)$$

$$Z_{\text{resid}} = Z - Z_{\text{trend}} \quad (6)$$

where Z_{trend} is the measured concentration, d is depth, and Z_{resid} represents the residuals used for variogram analysis. The coefficients k_0, k_1, and k_2 are the constant, linear, and quadratic regression terms estimated from the data. This detrending ensures that the vertical variogram captures local stratigraphic heterogeneity, not systematic depth gradients. Detrending was only implemented for varigram analysis purposes but was not on the original dataset to keep all the variability in the raw datasets.

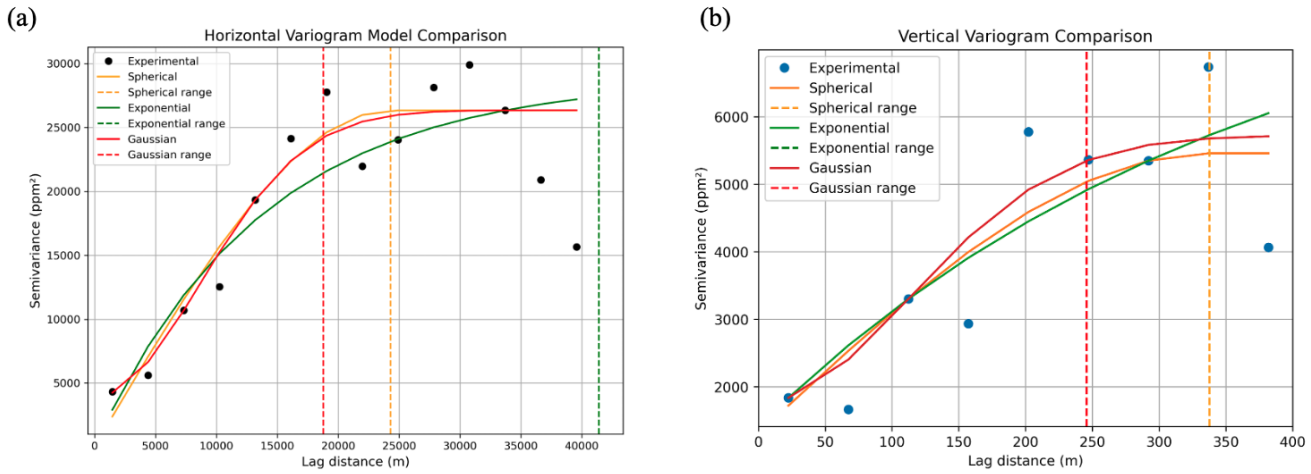

Figure 3: Experimental semi variograms and fitted theoretical models describing the spatial variability of lithium concentrations in the Smackover Formation. The left panel (a) shows lateral variance while the right panel (b) shows vertical variance over different lag distance or range.

3.2 Inverse Distance Weighting (IDW) Interpolation Method

IDW interpolation was used to construct a continuous 3D lithium concentration volume from the discrete brine samples (Shepard, 1968; Lu & Wong, 2008). IDW is a deterministic spatial interpolation method that estimates values at unsampled locations (x_0, y_0, z_0) as a weighted average of surrounding observations, assigning greater influence on nearby data with diminishing influence over distance (Shepard, 1968; Lu & Wong, 2008). Unlike kriging, IDW does not require second-order stationarity assumptions and performs robustly when sample density is moderate, making it appropriate for the Smackover dataset, which contains 541 deep brine geochemical samples with irregular spacing in both horizontal and vertical directions. The weighted average of IDW can be expressed as:

$$Z(x_0, y_0, z_0) = \frac{\sum_{i=1}^{N} w_i(x_0,y_0,z_0) v_i}{\sum_{i=1}^{N} w_i(x_0,y_0,z_0)} \quad (7)$$

where the weights (w_i) are based on the inverse of a distance metric that incorporates vertical anisotropy (Isaaks & Srivastava, 1989):

$$w_i(x_0, y_0, z_0) = [(x_i - x_0)^2 + (y_i - y_0)^2 + (a_Z(z_i - z_0))^2]^{-1} \quad (8)$$

Here, Z_i is the lithium concentration at sample i and a_z is vertical scaling factor used to emphasize no differences (horizontal to vertical anisotropy factor), and N is the number of measurements within the search radius.

IDW was carried out in the model grids/cells comprising measured concentration values that are within the lateral distance of 10 km and vertical distance of 125 m. Nodes with no neighbors were excluded from interpolation. Lithium concentrations interpolated across the 3D reservoir grid were converted into in-place lithium mass by multiplying Li concentration (ppm) by the modeled brine volume of each grid block. This approach follows standard volumetric assessment procedures applied in subsurface fluid-mineral systems, where mass-in-place is computed prior to the application of recovery factors (Beckers & McCabe, 2019). A representative reservoir cell volume (500 m × 500 m × 50 m) was used to quantify the total lithium contained within the fluid-filled portion of the Smackover Formation. This initial lithium mass estimate represents the total in-situ resource before accounting for geological and operational uncertainties.

3.3 Overview of the Analytic EGS Framework

To estimate the geothermal resource potential of the Smackover Formation, we adopt the 1D analytic fractured-reservoir framework presented by Burns et al. (2025). This formulation provides closed-form solutions for heat extraction from uniformly fractured reservoirs and for conductive recharge from surrounding rock. The analytical solutions employed here assume a constant heat extraction rate, providing an approximation of steady electrical output over the design lifetime of the power plant. From this formulation, the thermally affected region around the fracture network can be estimated, enabling calculation of the minimum allowable spacing between power plants and, in turn, the total EGS potential within the study area. In this conceptualization, the EGS reservoir is treated as a fractured volume with an effective fracture spacing that represents parallel flow paths between an injection and production well. Temperature within these fracture flow paths is assumed to be uniform, allowing heat transfer from the rock to be modeled as one-dimensional cooling at each fracture; the principle of superposition is then applied to estimate the combined cooling influence of many fractures. It further assumes that a power plant is designed to operate at a constant, sustainable heat production rate, consistent with a 30-year design life, so that electricity generation remains approximately steady and the plant can be sized for optimal efficiency. The 1-D conduction solution governing fracture-scale cooling is:

$$\Delta T(x,t) = \frac{2F_0^{\text{single}}}{\lambda}\left[\frac{\lambda t}{\Pi \rho c}^{1/2} e^{-\frac{\rho c x^2}{4\lambda t}} - \frac{x}{2}\text{erfc}\left(\frac{x}{2\left(\frac{\lambda t}{\rho c}\right)^{1/2}}\right)\right] \quad (9)$$

Here, λ is thermal conductivity, ρ is bulk density, c is specific heat capacity, t is the design lifetime, F_0^{single} is the single-fracture heat flux, x is the distance from the fracture, and $\Delta T(x,t)$ is the temperature drawdown from the initial uniform temperature with distance (x) from the fracture at time (t). We assumed heat extraction from parallel, evenly spaced fractures in an EGS reservoir. The power density (P) of a reservoir column is calculated as:

$$\int_{z(T<T_{min})} \varepsilon * \beta * 0.74 * \epsilon^{\text{lower}} * \left|\frac{\rho c \Delta T_0^{\text{design}}}{\Delta t_0^{\text{design}}}\right| dz < P < \int_{z(T<T_{min})} \varepsilon * \beta * 0.74 * \epsilon^{\text{upper}} * \left|\frac{\rho c \Delta T_0^{\text{design}}}{\Delta t_0^{\text{design}}}\right| dz \quad (10)$$

where ε, β, ϵ^{lower}, and ϵ^{upper} represent heat extraction efficiency, geology success factor, heat extraction lower efficiency, and heat extraction higher efficiency. For the Smackover application, we treat these parameters as depth-uniform due to the absence of detailed 3D variability. Under these assumptions, Equation (10) simplifies to:

$$\varepsilon * \beta * 0.74 * \epsilon^{lower} \int_{z(T>T_{min})} \left|\frac{\rho c \Delta T_0^{design}}{\Delta t_0^{design}}\right| dz < P < \varepsilon * \beta * 0.74 * \epsilon^{upper} \int_{z(T>T_{min})} \left|\frac{\rho c \Delta T_0^{design}}{\Delta t_0^{design}}\right| dz \quad (11)$$

Here, T_{min} is 82°C (Sanyal & Butler, 2005), $\Delta T_0^{\text{design}}$ is variable and site dependent based on a continuous temperature map (Aljubran et al. 2024), $\Delta t_0^{\text{design}}$ is 30 yr, and 0.74 is the ratio for non-interfering spherical reservoirs.

3.4 Stochastic Simulations

For Li resource assessment, three key parameters, porosity, oil-water contact ratio, and recovery efficiency, were sampled using uniform distribution (Figure 4). Uniform distribution was chosen because of data scarcity on mean and standard deviation of sampled parameters in the study area. Porosity was sampled from a uniform distribution between 0.02 and 0.15, reflecting typical ranges reported for Smackover carbonate reservoirs (Figure 4(a)). The oil-water contact ratio (0.75-0.95) accounted for variations in hydrocarbon saturation, which reduces the effective brine-filled pore space available to host dissolved lithium (Figure 4(b)). These two parameters jointly define

the effective water-filled porosity controlling brine volume (Figure 4(c)). The range of recovery efficiency (50-75%) reflects an optimistic assumption given the expected technical and operational uncertainties associated with high-salinity brine extraction (Burns et al., 2025; Sayal et al., 2005; Williams, 2010), rather than a literature-prescribed standard (Figure 4(d)). Each parameter was sampled 250 times to represent the sampling space.

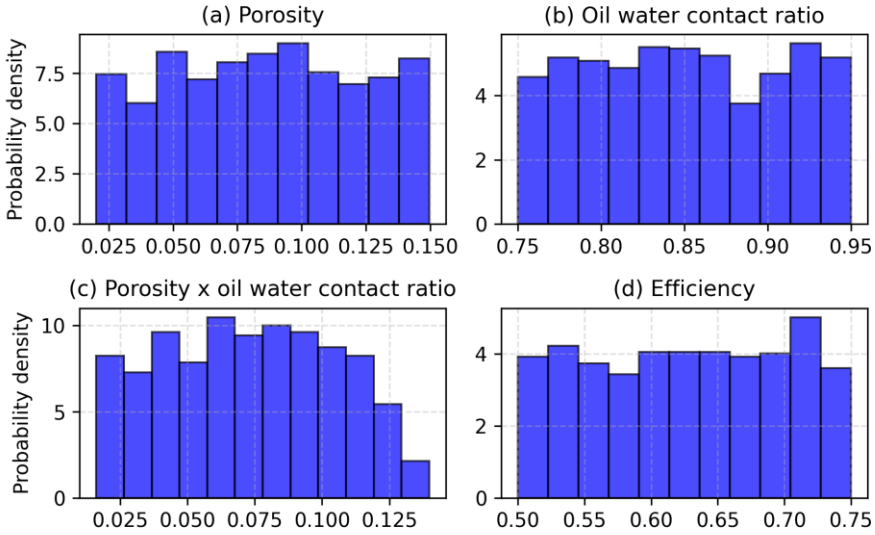

Figure 4: Uniform distribution of porosity (a), oil water contact (b), reduced porosity due to oil water contact (c), and Li extraction efficiency (d).

Seven key parameters were sampled to compute geothermal power density (Figure 5). The distributions represent the full stochastic sampling space used to evaluate geothermal power density in the northern Smackover Formation, capturing uncertainty across seven governing physical and operational parameters. The sampled ranges for thermal conductivity (2.5-3.0 $Wm^{-1}K^{-1}$), bulk density (2600-2800 kgm^{-3}), and specific heat capacity (750-850 $Jkg^{-1}K^{-1}$) fall within the experimentally established properties of sedimentary carbonates and dolomitized limestone and earlier geothermal property compilations for U.S. sedimentary basins (Robertson, 1988; Thomas et al., 1973). Temperature drawdown was varied from 30–60°C to encompass the operationally realistic cooling envelope for long-term EGS so that the reservoir does not fall below 82°C (Sanyal & Sarmiento, 2005, Alijubran et al., 2024). These distributions also include reservoir-scale variables, fracture spacing (10-30 m) and reservoir radius (300-600 m), which mirror the geometric assumptions widely adopted in analytical EGS models for stimulation spacing and conceptual well-pair configurations (Doe et al., 2014; Kumar et al., 2021; Wang et al., 2022; Zeinabady & Clarkson, 2024). Heat-to-electricity conversion efficiency (0.10-0.20) was sampled in our framework to bracket both typically observed performance of binary-cycle geothermal installations (Zarrouk & Moon, 2014; Dickson & Fanilli, 2003) and potential high-efficiency plant configurations under favorable thermodynamic conditions, e.g., optimized ORC cycles, (Merbecks et al., 2024). Finally, the geologic success factor, representing the fraction of reservoir volume that can be successfully stimulated and produced at economically meaningful flow rates, was sampled broadly (0.05-0.90) to reflect the large uncertainty in reservoir continuity, fracture connectivity, and long-term sustainability as discussed in recent probability-of-success studies for geothermal reservoirs (Schumacher et al., 2020; Dekkers & de Pater, 2022). Each of 250 samples was analyzed on each model grid (16 by 8), requiring a total of 24,000 model runs.

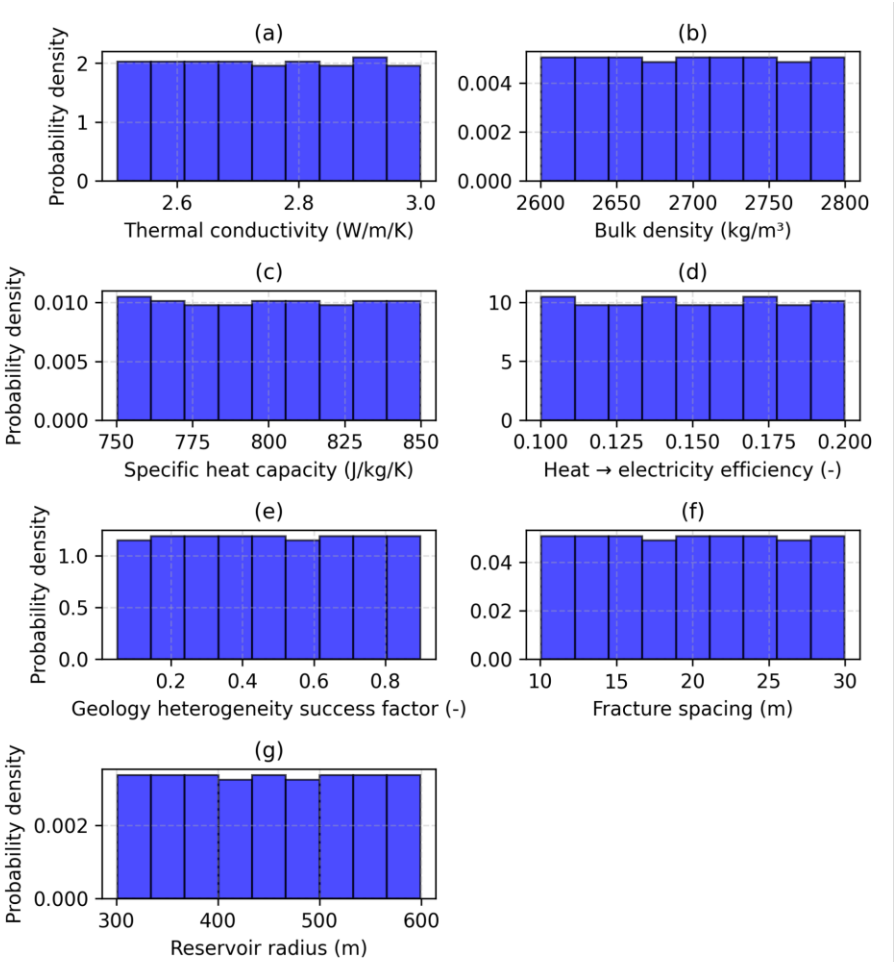

Figure 5: Uniform distribution of seven parameters (a–g) used to compute geothermal power density. Only minimum and maximum values were used to generate a total of 250 samples for each parameter.

4. RESULTS

Lithium resource estimation across the northern Smackover indicates that elevated concentrations are primarily within the deeper portions of the formation, consistent with the subsurface geochemical trends observed in brine sampling campaigns (Figure 6). The spatial distribution analysis shows that areas with sparse data coverage exhibit greater uncertainty, particularly where lithologic and structural heterogeneity influence reservoir continuity. By integrating lateral and vertical variability through geostatistical modeling, a volumetric calculation of lithium in place was achieved for the entire modeled domain. This analysis yielded an estimated total subsurface lithium mass of approximately seven million tonnes distributed across ~770 km³ of reservoir volume. The resulting spatial lithium map reflects both the strong geological controls on brine chemistry and the limitations imposed by measurement sparsity.

When recovery efficiencies, brine production parameters, and lithium extraction factors were incorporated, only a small proportion of the total subsurface lithium volume was assessed to be realistically recoverable. The stochastic modeling framework produced a mean recoverable estimate near 0.3 million tonnes (Figure 7), implying an approximate efficiency of just over four percent. This reduced value is driven largely by low porosity, high oil water contact, practical extraction limits, and the heterogeneous distribution of lithium-enriched intervals within the reservoir. The resulting distribution of recoverable mass reveals a strongly right-skewed behavior, reflecting the dominance of a few high-grade zones over a broad region of lower concentrations. These findings emphasize that while the lithium amount is geologically significant, its practical exploitation is constrained by both reservoir quality and extraction efficiency.

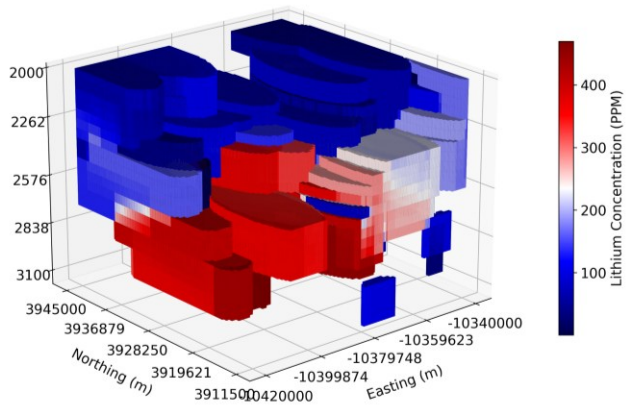

Figure 6: Lithium concentration within the selected model domain. No proximal samples within the horizontal (10 km) and vertical (125 m) search criteria were left uninterpolated and shown in transparent portions.

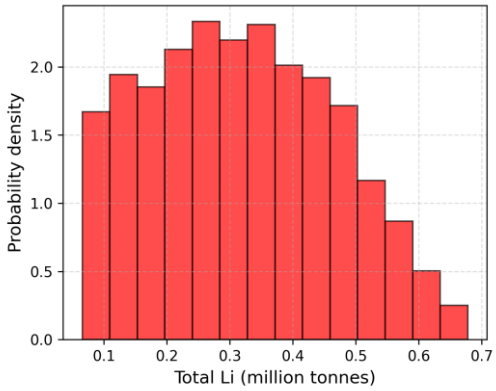

Figure 7: Total Li concentration distribution in the selected model domain. PDF of total recoverable lithium (million tonnes) derived from 1,000 Monte Carlo realizations incorporating porosity, brine saturation, and recovery efficiency uncertainties.

Thermal gradient was computed using a Stanford geothermal model (Aljubran et al., 2024), and formation temperatures were subsequently estimated at depths of 2300 m and 2600 m (Figure 8). Thermal drawdown across the study region ranges between approximately 12 and 21 °C, with the highest drawdown concentrated near the central portion of the modeled area and gradually decreasing toward the margins. The contour map illustrates a coherent spatial pattern in which warmer zones form elliptical clusters in the interior, reflecting localized thermal anomalies or variations in heat flow. Cooler drawdown regions appear along the western and eastern edges, suggesting lateral gradients in reservoir temperature or thermal conductivity. This heterogeneous thermal structure of the northern Smackover Formation was passed to Equation 11 for computing geothermal power density, thermodynamic maximum power density and corresponding higher and lower bounds.

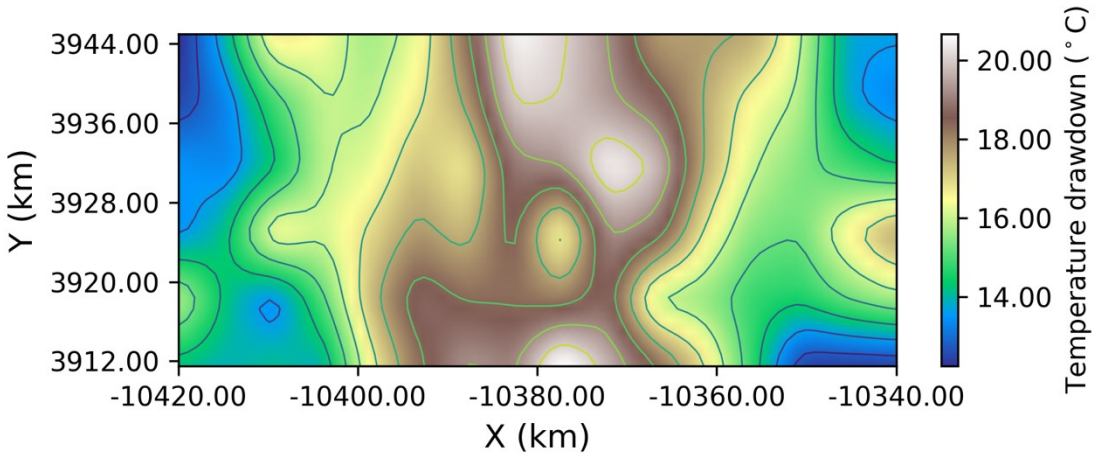

Figure 8: Temperature drawdown map at 2600 m depth in the study area demonstrates how much power we can extract between 2300 m to 2600 m depth.

Geothermal power density estimation using analytical EGS formulations yields clear distinctions between thermodynamic and realistic performance bounds (Figure 9). The thermodynamically maximum power density across the modeled region averages roughly 11 W/m^2, ranging between ~8 to ~14 W/m^2 (Figure 9(c)). These values are based on formation temperature drawdown and conductive heat recharge potential at depth. These upper-bound values reflect the ideal limit in which all accessible heat is converted without operational losses. In contrast, scenarios incorporating realistic efficiency factors, including geologic success probability and heat-to-electricity conversion, produce markedly lower outcomes. The mean realistic minimum and maximum power densities cluster around 0.48-0.86 W/m^2 (Figures 9-10), illustrating that operational constraints dominate the practical energy yield.

The narrow gap between realistic minimum and maximum estimates indicates that efficiency factors strongly compress the range of feasible outcomes. Even under optimistic parameter realizations, heat recovery limitations and low conversion efficiencies restrict the achievable power density to well below the thermodynamic envelope. Spatial patterns in realistic power maps show consistent gradients tied to temperature drawdown behavior and reservoir geometry. The efficiency limit could not change the distribution because of constant

efficiency factors. The realistic thermal regime of the Smackover suggests that significant heat in place is present, yet only a small fraction is technically extractable via EGS without enhanced efficiencies.

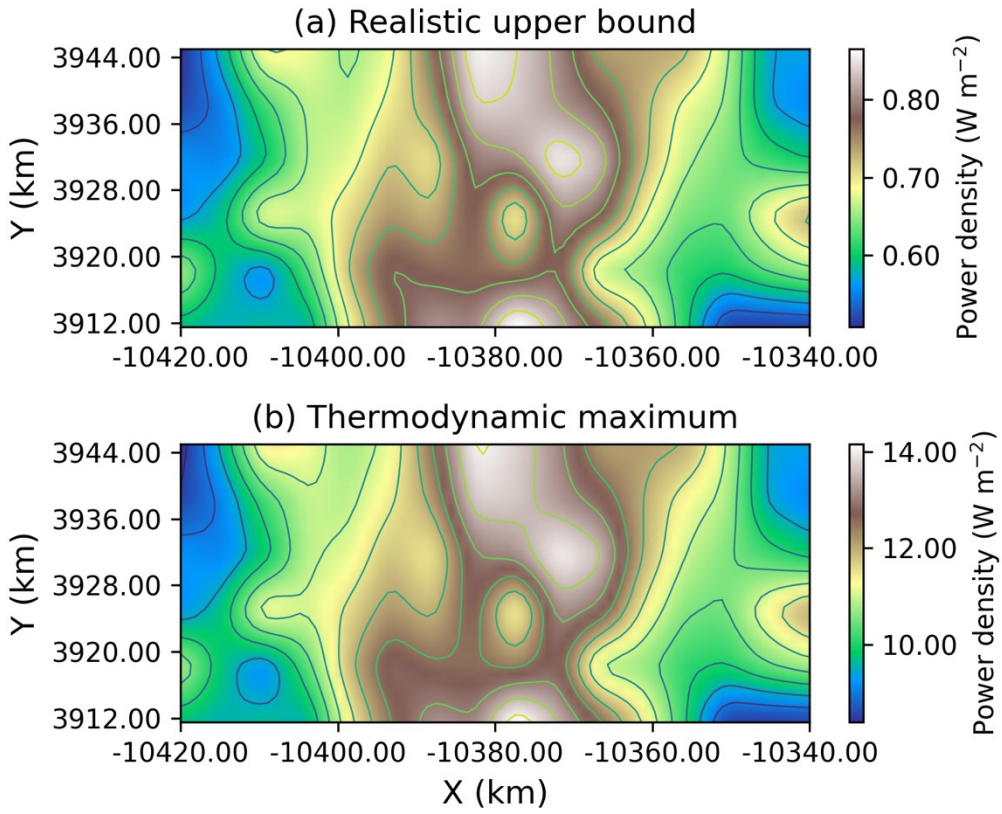

Figure 9: The mean realistic maximum power density in the study area (a); and the mean of thermodynamically maximum power density in the study area (b).

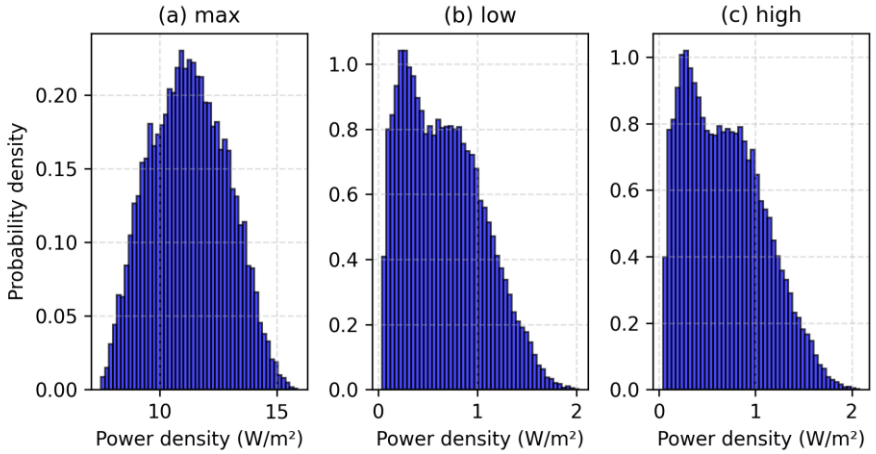

Figure 10: Potential geothermal power density distribution for thermodynamically maximum (a), low realistic minimum (b), and high realistic high (c).

Detailed probabilistic analysis reveals that geothermal power density is most sensitive to temperature drawdown assumptions and the geologic success factor, which together govern the sustained heat flux achievable during reservoir operation (Figure 10). The thermodynamically maximum power density spans from approximately 0.5 to 18 W/m² across realizations, reflecting the combined variability in rock thermal properties and reservoir dimensions (Figure 10(a)). These values mark the upper benchmark for heat extraction

before operational penalties are considered. Both the thermodynamically lower and upper bounds of power density span from approximately 0.1 to 2.1 W/m² across realizations (Figure 10(b)) and majority are skewed to lower values. The broad spread also highlights the variability induced by uncertain temperature gradients within the formation. Such variability is critical for future site prioritization, particularly in zones where temperature and efficiency data remain sparse.

In comparison, the distributions of realistic minimum and maximum power densities show limited divergence due to the dominant influence of low conversion efficiencies relative to the total heat in the reservoir (Figure 10(b-c)). Even when reservoir geometry and thermal conductivity values favor higher extraction, the achievable power remains sharply constrained by efficiency factors. The histogram distributions reveal strong clustering within the lower-power regime, especially when success probabilities are modest. This pattern suggests that improvements in the engineering aspects of EGS, rather than geological variability would have the greatest impact on increasing power output. Consequently, technological advancements in well stimulation and conversion systems are likely prerequisites for substantial geothermal deployment in this region.

These findings show that geological heat availability alone is insufficient to guarantee meaningful geothermal power recovery. Instead, realistic estimates require integrating operational constraints and efficiency assumptions directly into the heat extraction models. The probabilistic workflow demonstrates the degree to which uncertainty in fracture spacing, reservoir radius, and thermal drawdown collectively affect the recoverable energy. Despite this variability, the overall conclusion is that only a small proportion of the theoretical geothermal potential can currently be converted to electricity on a scale. This reinforces the need for co-optimization strategies that consider geothermal and lithium extraction jointly, as the combined value stream may enhance economic viability even when geothermal power density is modest.

5 Conclusions

The stochastic co-resource assessment shows that meaningful characterization of lithium and geothermal potential within the northern Smackover Formation is achievable even under sparse and uneven subsurface data conditions. By integrating variogram-based spatial continuity analysis with anisotropic 3D IDW interpolation, the lithium assessment captures both lateral and vertical heterogeneity in brine chemistry. The results reveal approximately seven million tonnes of total in-place lithium distributed across ~770 km³ of reservoir volume, with elevated concentrations occurring primarily at greater depths. However, the recoverable lithium fraction is significantly smaller, on the order of 0.3 million tonnes, largely due to low effective porosity, reduced brine-filled pore volume resulting from high oil-water contact ratios, and modest extraction efficiencies. These findings underscore the importance of accounting for reservoir quality and operational constraints when evaluating the economic feasibility of direct lithium extraction from subsurface brines.

The geothermal resource assessment demonstrates that the Smackover Formation contains modest theoretical heat in place and only a small fraction can be converted to useful power under realistic conditions. Analytical EGS modeling, incorporating seven key thermophysical, geometric, and efficiency parameters, reveals a clear disparity between thermodynamic potential and extractable power. While thermodynamically maximum power densities range from ~8 to 14 W m^{-2} across the study area, realistic power densities cluster narrowly between ~0.48 and 0.86 W m^{-2}. This reduction of outcomes is driven primarily by low heat-to-electricity efficiencies and limited geologic success factors rather than by the magnitude of available heat. The temperature drawdown map, characterized by 12–21°C of cooling between 2300 m and 2600 m, further shows that thermal heterogeneity influences spatial variations in power potential, but efficiency losses ultimately dominate practical outcomes.

Collectively, these results indicate that the northern Smackover Formation holds substantial Li potential and modest geothermal resources. However, neither resource is fully realizable without improvements in both geologic characterization and engineering capabilities. For lithium, more refined porosity and saturation data, along with enhanced DLE performance, are needed to improve recoverable estimates. For geothermal energy, advances in reservoir stimulation, fracture connectivity, and heat-conversion systems are essential to lift realistic power output closer to its thermodynamic ceiling. The stochastic framework applied here provides an integrated, uncertainty-aware evaluation of both commodities, demonstrating how joint assessment can better inform future exploration, development strategies, and techno-economic planning. Ultimately, the combined value of lithium extraction and geothermal heat recovery may provide synergistic pathways for resource co-development, even where each resource alone may face technical or economic limitations.

ACKNOWLEDGEMENTS

This work is financially supported by the LiGRAS project from the U.S. Department of Energy's Office of Geothermal. This paper describes objective technical results and analysis. Any subjective views or opinions that might be expressed in the paper do not necessarily represent the views of the U.S. Department of Energy or the United States Government. The authors also thank Erick R. Burns and Justin E. Birdwell of the U.S. Geological Survey for their valuable discussions, guidance, and data.

REFERENCES

Aljubran, M. J., & Horne, R. N. (2024). Thermal Earth Model for the Conterminous United States Using an Interpolative Physics-informed Graph Neural Network. *Geothermal Energy*, *12*(1), 25. https://doi.org/10.1186/s40517-024-00304-7.

Attanasi, E. D., Coburn, T. C., & Freeman, P. A. (2024). Machine Learning Approaches to Identify Lithium Concentration in Petroleum Produced Waters. Mineral Economics, 1-21.

Beckers, K. F., & McCabe, K. (2019). GEOPHIRES v2.0: Updated Geothermal Techno-economic Simulation Tool. *Geothermal Energy*, *7*(1). https://doi.org/10.1186/S40517-019-0119-6.

Blondes, M. S., Knierim, K. J., Croke, M. R., Freeman, P.A., Doolan, C., Herzberg, A.S., & Shelton, J.L. (2023). U.S. Geological Survey National Produced Waters Geochemical Database (ver. 3.0, December 2023): U.S. Geological Survey data release, https://doi.org/10.5066/P9DSRCZJ.

Burns, E. R., Zhang, J., Zhan, H., & Williams, C. F. (2025). Update of the 2008 Provisional Enhanced Geothermal Systems (EGS) Assessment for the Great Basin, USA. PROCEEDINGS, 50th Workshop on Geothermal Reservoir Engineering, Stanford University, Stanford, California, SGP-TR-229.

Cressie, N., & Hawkins, D. M. (1980). Robust Estimation of the Variogram: I. *Journal of the International Association for Mathematical Geology*, *12*(2), 115–125. https://doi.org/10.1007/BF01035243/METRICS.

Darvari, R., Nicot, J. P., Scanlon, B. R., Kyle, J. R., Elliott, B. A., & Uhlman, K. (2024). Controls on Lithium Content of Oilfield Waters in Texas and Neighboring States (USA). Journal of Geochemical Exploration, 257, 107363.

Dickinson, K. A. (1968). *Upper Jurassic stratigraphy of some adjacent parts of Texas, Louisiana, and Arkansas*. US Government Printing Office.

Dickson, M.H., Fanelli, M., 2003. Geothermal Energy: Utilization and Technology. Routledge, ISBN-10: 1844071847, ISBN-13: 978-1844071845.

Dixit, A., Mandal, A., & Ganguli, S. S. (2024). Reservoir Heterogeneity Analysis Using Multi-directional Textural Attributes from Deep Learning-based Enhanced Acoustic Impedance Inversion: A Study from Poseidon, NW Shelf Australia. *Energy Geoscience*, *5*(2), 100235. https://doi.org/10.1016/J.ENGEOS.2023.100235.

Doe, T., Mclaren, R., & Dershowitz, W. (2014). Discrete Fracture Network Simulations of Enhanced Geothermal Systems. *PROCEEDINGS, Thirty-Ninth Workshop on Geothermal Reservoir Engineering*.

Ester, M., Kriegel, H. P., Sander, J., & Xu, X. (1996). A Density-based Algorithm for Discovering Clusters in Large Spatial Databases with Noise. Retrieved on 10/12/2025 from www.aaai.org.

Executive Summary - Global Critical Minerals Outlook 2025 - Analysis - IEA. (2025). Retrieved 11/02/2025 from https://www.iea.org/reports/global-critical-minerals-outlook-2025/executive-summary.

Flexer, V., Baspineiro, C. F., & Galli, C. I. (2018). Lithium Recovery from Brines: A Vital Raw Material for Green Energies With a Potential Environmental Impact in its Mining and Processing. *Science of The Total Environment*, *639*, 1188–1204. https://doi.org/10.1016/J.SCITOTENV.2018.05.223.

Gardner, R., and Birdwell, J.E. "Potential for co-production of lithium and geothermal resources in the U.S. Gulf Coast." GRC Transactions, 49, (2025), 410-418.

He, X., Kaur, S., & Kostecki, R. (2020). Mining Lithium from Seawater. *Joule*, *4*(7), 1357–1358. https://doi.org/10.1016/j.joule.2020.06.015.

Huang, X., Ahmmed, B., Mehana, M., Bhattacharya, S., & Neil, C. (2025). Data-driven Lithium and Geothermal Resource Assessment in the Smackover Formation. *PROCEEDINGS*, 50th Workshop on Geothermal Reservoir Engineering, Stanford University, Stanford, California.

Isaaks, E. H., & Svrivastava, R. (1989). An Introduction to Applied Geostatistics. *Oxford University Press*. Oxford University Press, Inc.

Journel, A. G., & Huijbregts, C. J. (1978). Mining Geostatistics. *Blackburn Press, 2003*. Blackburn Press. Retrieved on 12/16/2025 from https://books.google.com/books/about/Mining_Geostatistics.html?id=Id1GAAAAYAAJ.

Knierim, K. J., Blondes, M. S., Masterson, A., Freeman, P., McDevitt, B., Herzberg, A., Li P., Mills C., Doonal C., Jubb A. M., Ausbrooks S. M., & Chenault, J. (2024). Evaluation of the Lithium Resource in the Smackover Formation Brines of Southern Arkansas Using Machine Learning. Science Advances, 10(39), eadp8149.

Kumar, D., & Ghassemi, A. (2021). Modeling and Analysis of Multiple Hydraulic Fracturing Design in EGS. Proceedings World Geothermal Congress 2020+1.

Lu, G. Y., & Wong, D. W. (2008). An Adaptive Inverse-distance Weighting Spatial Interpolation Technique. *Computers & Geosciences*, *34*(9), 1044–1055. https://doi.org/10.1016/J.CAGEO.2007.07.010.

Madalimov, M., Li, D., Haynes, B., Dair, Y., Ehighebolo, I. T., & Ionescu, C. L. (2025). Heterogeneity Modeling and Heterogeneity-based Upscaling for Reservoir Characterization and Simulation. *SPE Journal*, *30*(02), 942–956. https://doi.org/10.2118/217511-PA.

Marza, M., Ferguson, G., Thorson, J., Barton, I., Kim, J. H., Ma, L., & McIntosh, J. (2024). Geological Controls on Lithium Production from Basinal Brines Across North America. Journal of Geochemical Exploration, 257, 107383.

Matheron, G. (1963). Principles of Geostatistics. *Economic Geology*, *58*(8), 1246–1266. https://doi.org/10.2113/GSECONGEO.58.8.1246.

Merbecks, T., Alfani, D., Bombarda, P., & Silva, P. (2024). On the Thermodynamic and Economic Performance of Binary Power Plant Configurations for the Exploitation of Two-phase Geothermal Resources. PROCEEDINGS, 49th Workshop on Geothermal Reservoir Engineering, Stanford University, Stanford, California, SGP-TR-227.

Moldovanyi, E. P., Walter, L. M., Brannon, J. C., & Podosek, F. A. (1992). New Constraints on Carbonate Diagenesis from Integrated Sr and S Isotopic and Rare Earth Element Data, Jurassic Smackover Formation, U.S. Gulf Coast: a reply. *Applied Geochemistry*, *7*(1), 93–97. https://doi.org/10.1016/0883-2927(92)90018-X.

Munk, L. A., Hynek, S. A., Bradley, D. C., Boutt, D., Labay, K., & Jochens, H. (2016). Lithium Brines: A Global Perspective. *Rare Earth and Critical Elements in Ore Deposits*. https://doi.org/10.5382/REV.18.14.

Nondorf, L. M. (2016). Thermal Conductivity, Thermal Gradient, and Heat-flow Estimations for the Smackover Formation, Southwest Arkansas. *Special Paper of the Geological Society of America*, *519*, 95–114. https://doi.org/10.1130/2016.2519(07).

Peng Li. (2023). Smackover Formation Lithium Update for 2021. *Arkansas Geological Survey*. Retrieved on 12/16/2025 from https://sedar.com/DisplayCompanyDocuments.do?lang=EN&issuerNo=00012543.

Robertson, E. C. (1988). Thermal Properties of Rocks. *U.S. Geological Survey*, *Open-File Report*(88–441).

Ruberti, M. (2024). Pathways to Greener Primary Lithium Extraction for a Really Sustainable Energy Transition: Environmental Challenges and Pioneering Innovations. *Sustainability 2025, Vol. 17, Page 160*, *17*(1), 160. https://doi.org/10.3390/SU17010160.

Sanyal, S. K., & Butler, S. J. (2005). An analysis of power generation prospects from enhanced geothermal systems. Geothermal Resources Council Transactions, 29, 131-8.

Sanyal, S.K., & Sarmiento, Z.F. (2005). Reporting Estimated Geothermal Resources. Proceedings, World Geothermal Congress.

Schumacher, S., Pierau, R., & Wirth, W. (2020). Probability of Success Studies for Geothermal Projects in Clastic Reservoirs: From Subsurface Data to Geological Risk Analysis. *Geothermics*, *83*. https://doi.org/10.1016/J.GEOTHERMICS.2019.101725.

Shepard, D. (1968). A Two-dimensional Interpolation Function for Irregularly-spaced Data. *Proceedings of the 1968 23rd ACM National Conference, ACM 1968*, 517–524. https://doi.org/10.1145/800186.810616.

Swain, B. (2017). Recovery and Recycling of Lithium: A Review. *Separation and Purification Technology*, *172*, 388–403. https://doi.org/10.1016/J.SEPPUR.2016.08.031.

Thomas, J., Frost, R. R., & Harvey, R. D. (1973). Thermal Conductivity of Carbonate Rocks. *Engineering Geology*, *7*(1), 3–12. https://doi.org/10.1016/0013-7952(73)90003-3.

U.S. Department Of Energy. (2024). 2021-2024 Four-year Review of Supply Chains for the Advanced Batteries Sector.

U. S. Geological Survey (2024). Mineral Commodity Summaries 2024. *Mineral Commodity Summaries*. https://doi.org/10.3133/MCS2024.

Wang, G., Ma, X., Song, X., & Li, G. (2022). Modeling Flow and Heat Transfer of Fractured Reservoir: Implications for a Multi-fracture Enhanced Geothermal System. *Journal of Cleaner Production*, *365*, 132708. https://doi.org/10.1016/J.JCLEPRO.2022.132708.

Williams, C. F. (2010). Challenges in the assessment and classification of enhanced/engineered geothermal system resources. Transactions-Geothermal Resources Council, 34, 449-453.

Zarrouk, S. J., & Moon, H. (2014). Efficiency of Geothermal Power Plants: A Worldwide Review. *Geothermics*, *51*, 142–153. https://doi.org/10.1016/J.GEOTHERMICS.2013.11.001.

Zeinabady, D., & Clarkson, C. R. (2024). Reservoir and Fracture Characterization for Enhanced Geothermal Systems: A Case Study Using Multifractured Wells at the Utah Frontier Observatory for Research in Geothermal Energy Site. *SPE Journal*, *29*(01), 592–605. https://doi.org/10.2118/217438-PA.

Zhang, G., Li, Y., Guan, X., Hu, G., Su, H., Xu, X., et al. (2024). Spontaneous Lithium Extraction and Enrichment from Brine with Net Energy Output Driven by Counter-ion Gradients. *Nature Water*, *2*, 1091–1101. https://doi.org/10.1038/s44221-024-00326-2.